AD-A173 188 CRYOGENIC ACOUSTIC MICROSCOPY(U) STANFORD UNIV CA 1/1
EDWARD L GINZTON LAB OF PHYSICS C F QUATE JUL 86
GL-4068 AFOSR-TR-86-0832 AFOSR-85-0168

UNCLASSIFIED F/G 14/2 NL

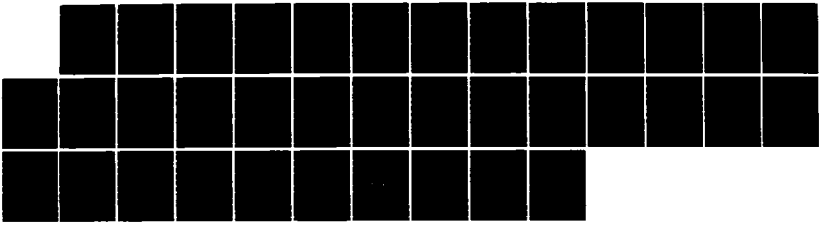

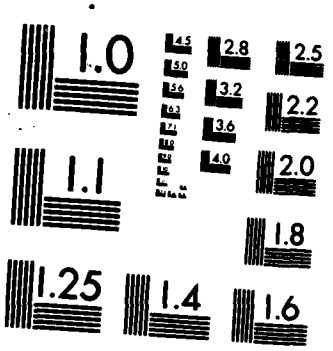

Edward L. Ginzton Laboratory
W. W. Hansen Laboratories of Physics
Stanford University
Stanford, California 94305

CRYOGENIC ACOUSTIC MICROSCOPY

Annual Technical Report

for the period

April 1, 1985 - March 31, 1986

Grant No. AFOSR-85-0168

The views and conclusions contained in this document are those of the authors and should not be interpreted as necessarily representing the official policies or endorsements, either expressed or implied, of the Air Force Office of Scientific Research or the U.S. Government.

Principal Investigator:

C. F. Quate

Professor of Applied Physics
and Electrical Engineering
Stanford University

G.L. Report No. 4068

July 1986

UNCLASSIFIED

SECURITY CLASSIFICATION OF THIS PAGE

AD-A173188

REPORT DOCUMENTATION PAGE

1a. REPORT SECURITY CLASSIFICATION: Unclassified	1b. RESTRICTIVE MARKINGS
2a. SECURITY CLASSIFICATION AUTHORITY	3. DISTRIBUTION/AVAILABILITY OF REPORT: Approved for public release; distribution unlimited.
2b. DECLASSIFICATION/DOWNGRADING SCHEDULE	
4. PERFORMING ORGANIZATION REPORT NUMBER(S): G.L. Report No.	5. MONITORING ORGANIZATION REPORT NUMBER(S): AFOSR-TR- 86-0832
6a. NAME OF PERFORMING ORGANIZATION: Stanford University, Edward L. Ginzton Laboratory; 6b. OFFICE SYMBOL (If applicable)	7a. NAME OF MONITORING ORGANIZATION: AFOSR/NE
6c. ADDRESS (City, State and ZIP Code): Stanford University, Stanford, California 94305	7b. ADDRESS (City, State and ZIP Code): Building 410, Bolling AFB, DC 20332-6448
8a. NAME OF FUNDING/SPONSORING ORGANIZATION: AFOSR; 8b. OFFICE SYMBOL (If applicable): NE	9. PROCUREMENT INSTRUMENT IDENTIFICATION NUMBER: AFOSR-85-0168
8c. ADDRESS (City, State and ZIP Code): Bolling AFB, DC 20332-6448	10. SOURCE OF FUNDING NOS. — PROGRAM ELEMENT NO.: 61102F; PROJECT NO.: 2306; TASK NO.: A2; WORK UNIT NO.:
11. TITLE (Include Security Classification): Cryogenic Acoustic Microscopy	
12. PERSONAL AUTHOR(S): Hadimioglu, B., and Quate, C. F.	
13a. TYPE OF REPORT: Annual; 13b. TIME COVERED: FROM 4/1/85 TO 3/31/86	14. DATE OF REPORT (Yr., Mo., Day): July 1986; 15. PAGE COUNT: 35
16. SUPPLEMENTARY NOTATION	

17. COSATI CODES			18. SUBJECT TERMS (Continue on reverse if necessary and identify by block number)
FIELD	GROUP	SUB. GR.	Acoustic microscopy Superfluid helium Sound waves

19. ABSTRACT (Continue on reverse if necessary and identify by block number)

The progress on the ultra-high resolution acoustic microscope is described. Two main areas are investigated: signal-to-noise ratio and a mechanical scanner. The signal-to-noise ratio (SNR) is improved by developing higher efficiency acoustic transducers for generating coherent sound and superconducting bolometers for broadband detection of sound. Some experiments to understand the effects of pressurizing liquid helium on the propagation of high intensity focused sound waves in superfluid helium are described. The possibility of utilizing parametric amplification of sound in liquid helium to improve the SNR is reported. Finally, the design and development of a new scanner which will have a wider scanning range with great precision operating in pressurized liquid helium are also described.

20. DISTRIBUTION/AVAILABILITY OF ABSTRACT: UNCLASSIFIED/UNLIMITED ☒ SAME AS RPT. ☐ DTIC USERS ☐	21. ABSTRACT SECURITY CLASSIFICATION: Unclassified
22a. NAME OF RESPONSIBLE INDIVIDUAL: ~~C. F. Quate~~ Maj. Joseph W. Hager	22b. TELEPHONE NUMBER (Include Area Code): ~~(415) 723-0213~~ (202) 767-4933; 22c. OFFICE SYMBOL: NE

DD FORM 1473, 83 APR — EDITION OF 1 JAN 73 IS OBSOLETE.

86 10

Unclassified

SECURITY CLASSIFICATION OF THIS PAGE

CRYOGENIC ACOUSTIC MICROSCOPY

April 1, 1985 - March 31, 1986

In this report we will report our progress on the ultra-high resolution acoustic microscope at Stanford. We have concentrated our efforts on two areas. We want to improve the signal-to-noise ratio of the microscope by improving the high efficiency acoustic transducers for generating coherent sound and superconducting bolometers for broadband detection of sound. We have performed experiments to understand the effects of pressurizing liquid helium on the propagation of high intensity focused sound waves in superfluid helium. We have worked on a system that utilizes parametric amplification of sound in liquid helium to improve the receiver noise performance of the microscope. Finally, we are developing a new scanner which will enable us to scan over wide areas in pressurized liquid helium with great precision.

I. RESEARCH ON SIGNAL-TO-NOISE RATIO IMPROVEMENTS

We first report on the research aimed at improving the signal-to-noise ratio of the microscope. Signal-to-noise is the key consideration as we go to higher frequencies for imaging with the highest resolution. The electrical and acoustic losses in the system increase and image quality suffers and this must be overcome by enhancing the signal-to-noise ratio (SNR). Improvement on the SNR is also needed to obtain good quality images of samples with very rough surfaces which scatter most of the sound waves to decrease the received signal.

Improvements on signal-to-noise ratio can come from four areas: 1) transducer design, 2) superconducting bolometers for broadband detection of sound, 3) the application of high pressure to the superfluid helium, which allows

larger acoustic signals to be transmitted through helium, and 4) the parametric amplification of sound waves in liquid helium to lower the receiver noise of the microscope.

A. Transducer Design

The transducer geometry used in the acoustic microscope consists of a thin-film piezoelectric layer sandwiched between two metal electrodes (usually gold) deposited on a sapphire rod. An rf-voltage is applied between the electrodes to create an electric field in the piezoelectric layer which generates plane longitudinal sound waves propagating in the sapphire rod. The piezoelectric layer usually used in the microscope is ZnO because of its high electromechanical coupling coefficient. The thickness of the ZnO layer is somewhere between a quarter and a half-wavelength to get optimum conversion efficiency and bandwidth. These thickness values correspond to 4000 Å and 8000 Å, respectively, at 4 GHz. Typical two-way conversion loss values of 12-14 dB have been measured at frequencies near 4 GHz with ZnO transducers. As we go to higher frequencies in order to improve the resolution, we encounter two problems. The first is that as the wavelengths of the acoustic waves becomes shorter and shorter, the required piezoelectric film becomes extremely thin. We often find electrical shorts between the metal electrodes of the transducer. The reason for these shorts is most probably pinholes in the ZnO layer. We have observed electrical shorts when high rf-fields were applied on the transducers fabricated between 4 and 8 GHz. Above 8 GHz, when the ZnO is less than 2000 Å thick, we measured electric shorts on approximately 75% of the transducers.

The second problem using the single ZnO layers as the transducer element is that the conversion efficiency becomes quite low at frequencies higher than 8 GHz. This is because of the low radiation resistance of the transducer structure. In analogy to electrical antennas, the acoustic radiation from the

transducer can be modeled as a radiation resistance for the electrical input port. At frequencies above 8 GHz this resistance becomes very small, usually less than 0.1 Ω for transducer geometries reasonable to use in the acoustic microscope. Such low resistances are undesirable for two reasons. First, electrically matching the transducer to the 50 Ω impedance of coaxial cables or 400 Ω impedance of waveguides is very difficult and it is narrowband. Second, the presence of electrical losses in the metal electrodes and the electrical matching network causes the conversion efficiency to become very low. As an example, the radiation resistance of a 125 μm radius transducer is only 0.06 Ω at a frequency of 8 GHz. The resultant two-way conversion loss values were measured to be around 30 dB at 8 GHz and at liquid helium temperatures. Operating at liquid helium temperatures with superconducting niobium top-electrodes reduced the loss to 20 dB. But even this value was considerably high as compared to low frequency operation because of the low radiation resistance of the transducer.

To overcome the problems mentioned above, we are now investigating a multi-layered transducer structure. This is made by depositing half-wave thick layers of two materials with different piezoelectric coupling coefficients one after the other and forming a kind of acoustic resonator. If the difference in the piezoelectric coupling constants of the two materials is large, it is possible to get a considerable increase in the radiation resistance as compared to single films by depositing a large number of layers. Unfortunately, along with increased radiation resistance comes reduced acoustic bandwidth. But the bandwidth is not an important problem as usually less than 1% bandwidth is required in the helium acoustic microscope.

We are working on three fronts to fabricate multi-layered transducer configuration: half-wave thick films of ZnO with alternate crystal structure, and two different structures of GaAs grown with molecular beam epitaxy (MBE).

ZnO is desirable to use in the multi-layered transducers because of its very high electromechanical coupling constant. If one uses a material with low coupling constant as the alternate layer, it is possible to obtain a reasonably high radiation resistance with a relatively small number of layers. There is one constraint on the transducer fabrication, however, namely, the whole deposition should be done in one single pump-down. This is required for several reasons; ease of fabrication, preventing the transducer from getting dirty by exposure to air, and also preventing any adhesion problems in the multi-layered structure. Currently we deposit ZnO by sputtering from a zinc target in an argon-oxygen atmosphere in a vacuum station dedicated to ZnO growth. Therefore, it is not possible to introduce materials other than the ones mentioned above in the station without contaminating the sputtering system.

Our first attempt to grow a multi-layered ZnO transducer structure centered on using zinc as the alternate layer. We tried to grow zinc layers in the ZnO station simply by changing the deposition conditions. We increased the rf-power in the sputtering station to increase the deposition rate and possibly to decrease the zinc-oxygen combination rate to get zinc-rich layers. But single films that we obtained in this way were not significantly different from our normal ZnO layers. They showed very low electrical conductivity and high acoustic power generation.

After the failure of our initial attempts to grow zinc in the zinc-oxide station, we turned our attention to a second technique for fabricating a multi-layered transducer using ZnO, by modulating the crystal structure. The optimum coupling between electrical signal and longitudinal acoustic waves in the hexagonal ZnO crystal is obtained when the c-axis of ZnO is oriented parallel to electric field and normal to the substrate. As the c-axis is rotated from the normal direction, acoustic coupling becomes weaker. In fact, the longitudinal coupling coefficient is zero when the angle between the c-axis and

electric field is 40°.

We have analyzed the multi-layered ZnO transducer structure using the Mason's model for the piezoelectric layers. Figure 1 clearly shows the improvement in the transducer performance when a multi-layered system is employed. The two-way tuned conversion loss of a transducer that consists of alternating ZnO layers with electromechanical coupling constants of 0.2 and 0.15 is plotted as a function of frequency in this figure. The remaining transducer parameters are as follows:

Transducer radius: 125 μm
Top-electrode: 2000 Å gold
ZnO thickness: Each layer 4000 Å (half-wave at 8 GHz) thick
Counter-electrode: 2000 Å gold
Substrate: sapphire
Series resistance: 1 Ω
Total number of ZnO layers: 13

As a comparison, conversion loss of a single ZnO layer with a coupling constant of 0.2 is also plotted in Fig. 1. It can be seen that a significant improvement can be expected with the multi-layered structure.

It has been shown by J. Wang and K. Lakin[1] that it is possible to obtain thin ZnO films with c-axis oriented at a finite angle to the substrate. This is done by tilting the substrate in the ZnO station and moving it away from the center. We have tried to repeat their results and deposited ZnO films as mentioned above and compared the piezoelectric characterization of these films with those of normal oriented ZnO which is deposited at normal incidence in the middle of the station. We observed that the electromechanical coupling constant

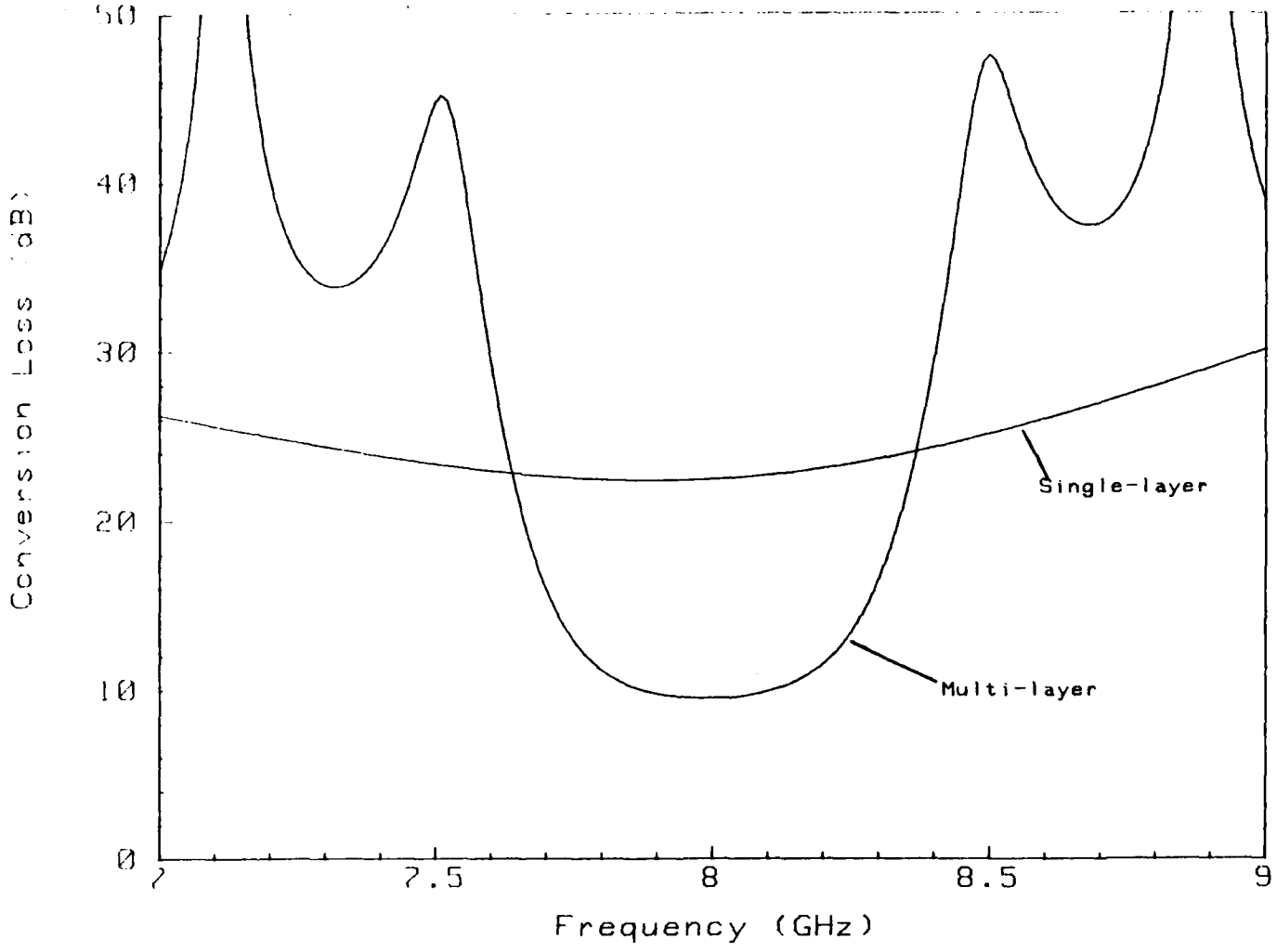

FIG. 1--Comparison of two-way theoretical conversion loss vs. frequency for multi-layer and single-layer transducers.

of the films does go down as the distance between the substrate and the center of the station is increased. We were successful in obtaining slanted ZnO layers with 50% lower coupling coefficient as compared to that of normally grown ZnO layers.

The next step in growing the multi-layered ZnO transducers was to grow the normal and tilted layers one after the other for different deposition conditions and measure the acoustical characteristics of the structure. Figure 2 shows a diagram of the set-up for the deposition of multi-layered ZnO structures. The substrate holder in the basic ZnO station is replaced by a system that can position the substrates at 3 locations. At position I, the pieces are normal to ZnO flow and in the middle of the station to deposit "normal" ZnO with high piezoelectric coupling coefficient. At positions II and III the pieces are moved a distance d from the center of the station and tilted 40° with respect to ZnO flow. At these positions we expect to grow ZnO with lower piezoelectric coupling constant. The holder is moved between positions I, II and III to deposit the multi-layered transducers.

We have made several multi-layered ZnO depositions with this setup to determine optimum system configuration for best ZnO growth. We have found that the distance, d , between the center of station and the substrates at the tilted position is especially important in determining the acoustic characteristics of the transducers. When d is less than 1", tilted films have characteristics close to normal ZnO. The resultant structures behave like a single thick film of ZnO. When d is greater than 2" we have found that after growing 2 or 3 half-wave layers the remaining layers grow with randomly oriented grains. The top surface shows roughness on the scale of 5-10 μm. The resultant transducers show very poor conversion efficiencies.

We have found in this way that a distance of 1.5" for d is probably the optimum location for the growth of multi-layered transducers. The top surface

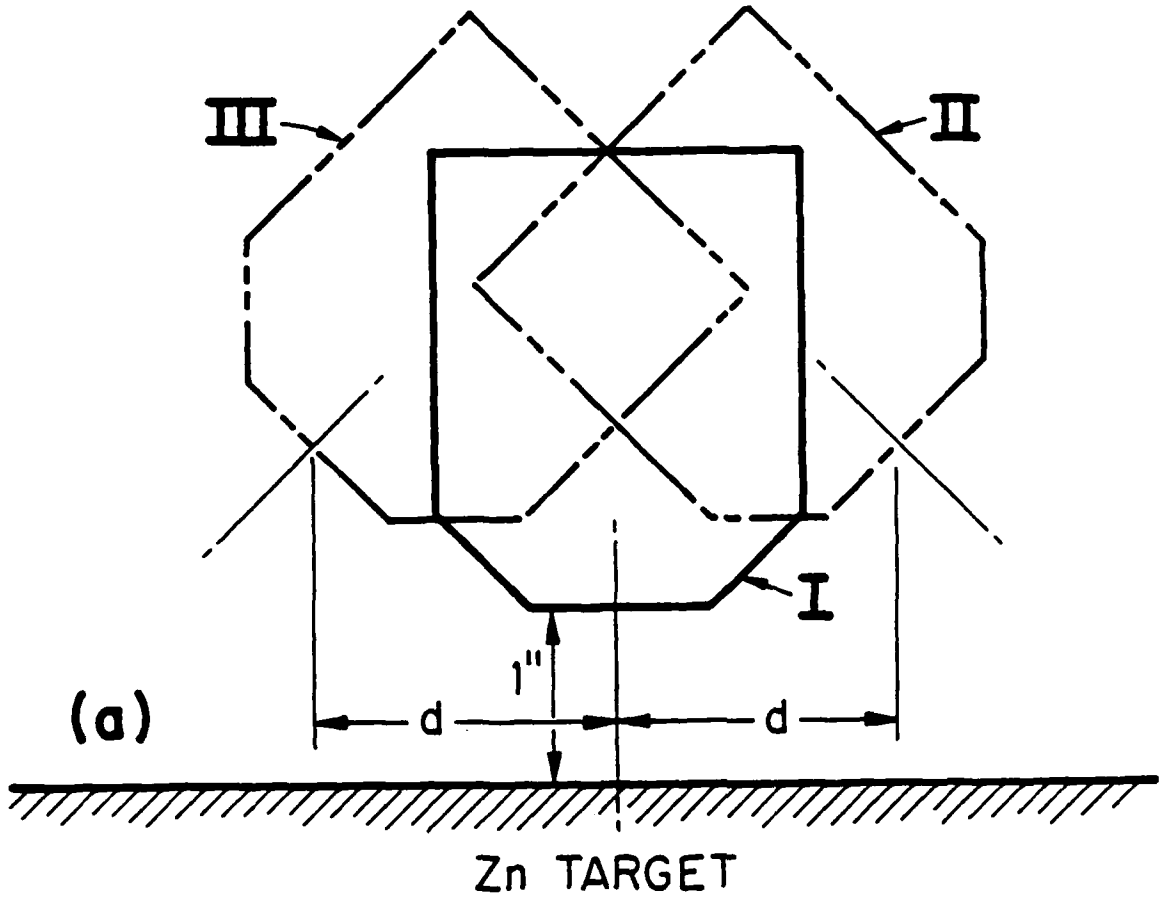

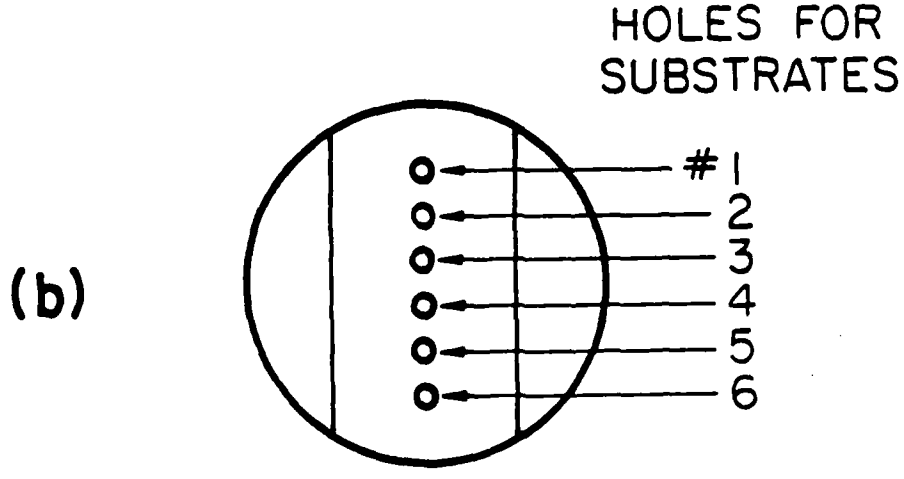

FIG. 2--(a) Diagram of the system used to deposit multi-layered ZnO transducers.
(b) Bottom view of the holder to place the substrates in the ZnO station.

of the resultant structures looks quite smooth under the scanning electron microscope. Although the pieces in the middle of the holder (#3 and #4 in Fig. 2) showed poor acoustic characteristics for reasons yet unknown, the remaining pieces had excellent responses. These are shown in Fig. 3. The two-way conversion loss of a multi-layered transducer operating at a temperature of 4K is plotted in this figure. The transducer parameters are listed below:

Center frequency:	8 GHz
ZnO thickness:	4000 Å (half-wave at 8 GHz)
Top-electrode:	2000 Å gold
Counter-electrode:	1000 Å gold
Transducer radius:	125 μm
Substrate:	sapphire
Total number of ZnO layers:	13 (7 normal, 6 tilted)
Substrate position (d):	1.5"
Substrate number:	6

The transducer was tuned for operation at 8 GHz in liquid helium. It can be seen that minimum conversion loss is only 12 dB with a bandwidth of approximately 200 MHz. As a comparison, the two-way conversion loss of a single ZnO layer operating in similar conditions is also plotted in Fig. 3. The loss of the single film is almost 20 dB worse as compared to the multi-layered case. It can also be seen that the bandwidths of the two transducers are approximately the same. This means that it is the electrical matching network that determines the bandwidth of the transducer, not the acoustical resonances in the ZnO layers, so the tuned multi-layered structures do not reduce the bandwidth.

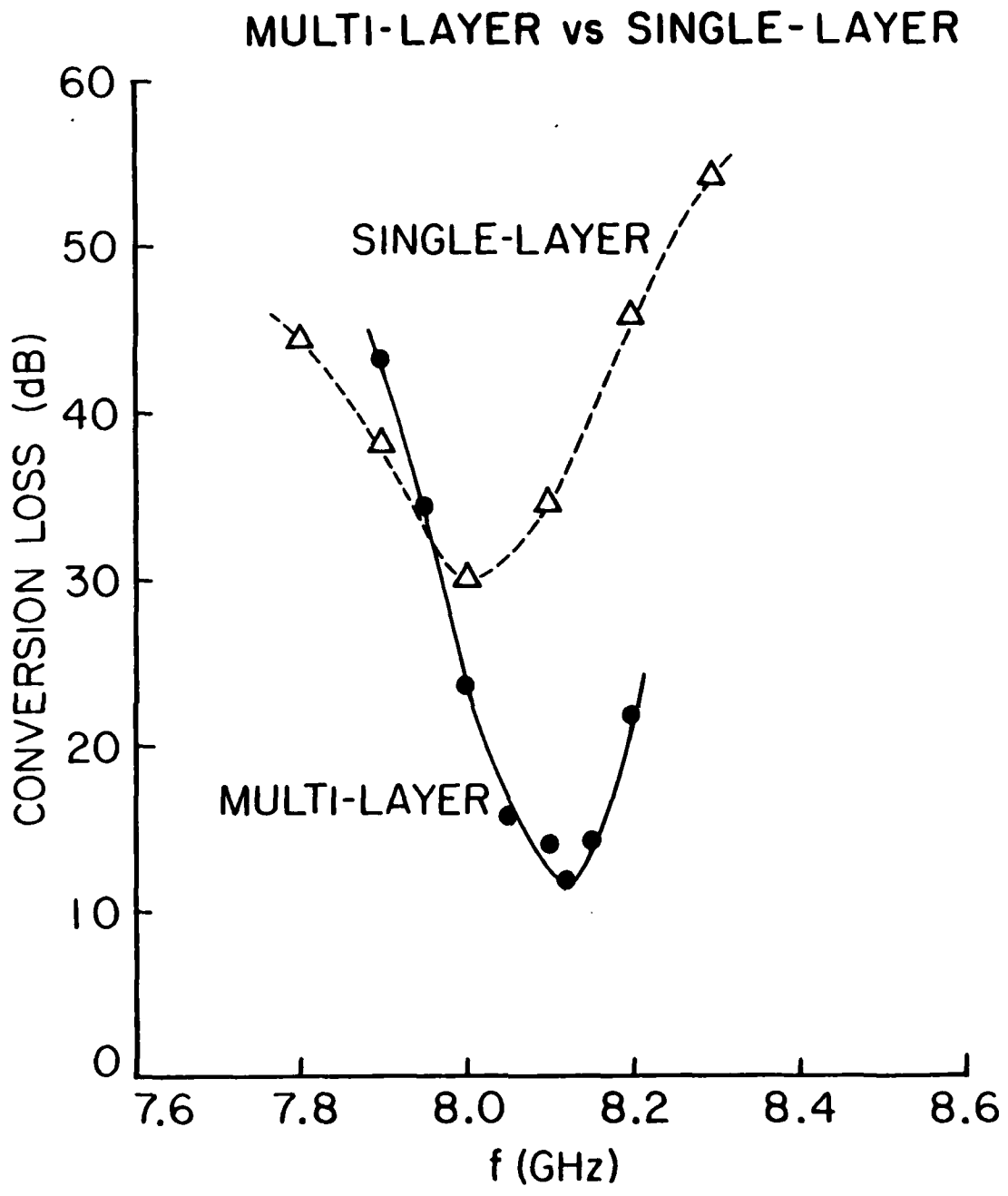

FIG. 3--The two-way tuned conversion loss of a multi-layer and a single-layer ZnO transducer operating in liquid helium.

S560.2

We are now in the process of fabricating multi-layered transducers at 12 GHz to determine their properties at higher frequencies. We will deposit niobium top-electrodes on these transducers to reduce the electrical losses at the lower temperatures. This should improve the conversion loss over that shown in Fig. 3.

We now believe that the multi-layered ZnO transducers with their increased efficiency will improve the signal-to-noise ratio and thus improve the image quality of the high resolution helium acoustic microscope. They will also enable us to go to much higher frequencies and to image with even higher resolution.

There is one problem, however, with the multi-layered ZnO transducers. That is the deposited ZnO layers are not perfect crystals as evidenced by the presence of pinhole defects in the thin-films and grainy appearance of the ZnO under the scanning electron microscope. Therefore, it may not be possible to get the improvement mentioned above at frequencies greater than 20 GHz when acoustic wavelengths become very short. It is possible, however, to obtain multi-layered transducers with near perfect crystal structures by using superlattices grown by molecular beam epitaxy (MBE). We have two different approaches to use these superlattices as transducer elements. In the first one we are fabricating superlattices of alternating layers of GaAs and $Al_{0.5}Ga_{0.5}As$ as shown in Fig. 4(a). These superlattices have been developed at various places before and shown to be almost defect-free even after deposition of more than 100 layers. There is one additional requirement, however, in our transducer application; the orientation of the layers should be such that <111> axis is normal to the substrate (parallel to electric field) compared to <100> axis commonly grown. This is required because there is no coupling between electric and acoustic fields when <100> axis of cubic GaAs crystal is parallel to electric field. Maximum longitudinal coupling coefficient is obtained when <111>

SUPERLATTICE TRANSDUCERS

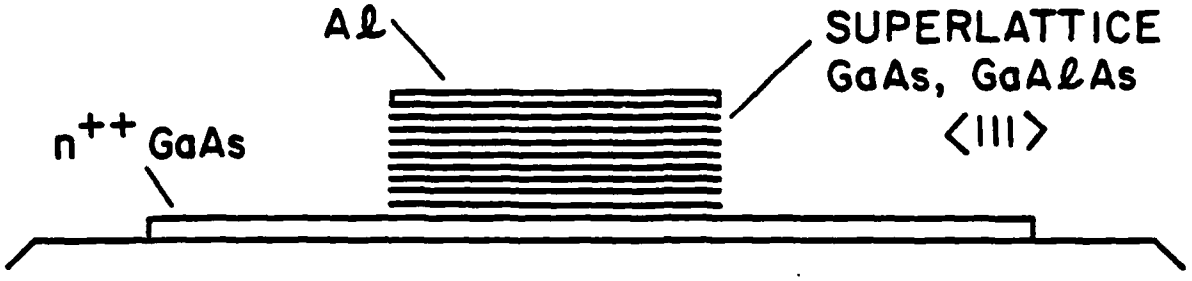

⟨111⟩ GaAs SUBSTRATE

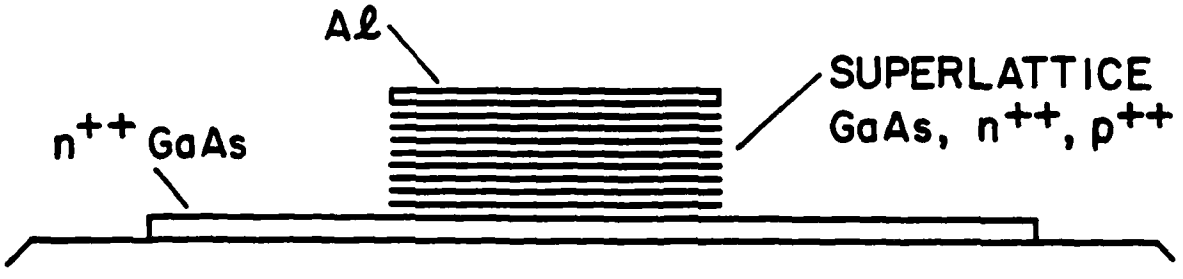

⟨100⟩ GaAs SUBSTRATE

FIG. 4--Configuration of superlattice transducers fabricated using molecular beam epitaxy.

(a) Alternating layers of <111> oriented GaAs and $Ga_{0.5}Al_{0.5}As$.

(b) Alternating layers of p and n doped <100> GaAs.

axis is parallel to the applied electric field. Since the piezoelectric coupling constants of the GaAs and $Ga_{0.5}Al_{0.5}As$ are very close to each other (0.062 and 0.078, respectively) up to 100 layers have to be grown in order to bring the radiation resistance up to a reasonable value of 0.1 Ω. Because of the limited MBE facilities we presently have available, we are attempting to have these superlattices made at AT&T by Art Gossard, as shown in Fig. 4(a). The aluminum layer on the top and the heavily doped GaAs layer on the bottom of the structure will serve as top and counter-electrodes, respectively.

The second approach using the MBE technique in multi-layered transducers is to employ a structure shown in Fig. 2(b). In this technique alternating layers of heavily doped (approximately 10^{19} cm^{-3}) n and p GaAs are grown using MBE. In such a structure some space charge of opposing polarity is accumulated across the interface between each n and p doped layer. As described by Ruden and Döhler,[2] the application of an external electric field across the superlattice creates Coulomb forces between the space charges and these forces squeeze and expand the lattice as the polarity of the electric field is changed. Therefore, one obtains a sound wave at the frequency of the applied electric field. Since the direct piezoelectric coupling in GaAs is not used, GaAs can be grown with <100> axis normal to the substrate. These structures are of interest to Gottfreid Döhler at Hewlett-Packard and we are hoping to have them fabricated in that facility.

B. Bolometers for Incoherent Phonon Detection

The acoustic transducers previously mentioned detect sound waves coherently, that is, they respond to the phase and amplitude of the incident sound radiation. Another method of sound detection is to use a bolometer, which measures the incident energy of the sound without regard for coherence.

Thus the bolometer can be referred to as an incoherent phonon detector - it counts the number of incident phonons.

For use in superfluid helium, bolometers are typically made with materials where the resistance varies as a function of temperature. The sensitivity of the bolometer depends on the strength of the temperature dependence. For this reason, superconductors are often used for bolometers due to their extreme temperature sensitivity at the critical temperature that defines the superconducting transition. The operation of the superconducting bolometer is as follows: the superconductor is biased (either with temperature, current, or magnetic field) so that its resistance is on the low side of the resistive transition. If an acoustic pulse is incident on the superconductor it will warm slightly, causing the resistance to climb as the superconductor becomes more "normal." The resistance change can be measured by passing a constant current through the superconductor and measuring the change in voltage.

Bolometers could have two important uses for the acoustic microscope. First, because they are only energy sensitive, they are inherently broadband. The piezoelectric transducers we have described are generally narrowband. We know that the sound propagating in the superfluid helium used in the microscope tends to generate harmonics, but these are undetectable with our transducers because of bandwidth limitations. Incoherent bolometers should be able to detect the harmonics of the transmitted sound waves, adding to the received signal. There is another benefit from harmonic detection: direct improvement of the resolution of the microscope. This results because the harmonics focus to a smaller spot than the fundamental transmitted wave since their wavelengths are shorter.[3]

The second important use for bolometers is their potential signal-to-noise of detecting phonons relative to transducers. At the present time, transducers are a much more sensitive detector of coherent sound radiation than bolometers

for frequencies of 8 GHz and under. As we push to higher frequencies, however, transducers will be less efficient and bolometers may surpass them.

To begin our work on bolometers, we first visited V. Narayanamurti's laboratory at AT&T Bell Laboratories to learn their state-of-the-art bolometer/receiver methodology. Since then we have fabricated and demonstrated our own bolometers. An example of an experiment is shown in Fig. 5(a). The bolometer is a thin-film of aluminum, electron-beam deposited at room temperature with 20.10^{-6} torr of oxygen background pressure. The oxygen causes defects in the aluminum film and raises the critical temperature so that the bolometer can be tested in a simple pumped helium bath (T = 1.3 K). (The superconducting critical temperature for pure aluminum is about 1 K and goes up to 1.4 - 1.7 K with oxygen.) The aluminum bolometer in Fig. 5(a) has been deposited on a sapphire slab. On the opposite face of the slab, a thin-film of chrome (500 Å thick) has been deposited. When a current pulse is passed through the chrome, a pulse of thermal phonons is launched into the sapphire and can be detected by the bolometer as shown in the figure. Two thermal phonon pulses are actually detected because the longitudinal and transverse phonons separate in time due to their differing sound speeds. The data in Fig. 5(b) demonstrate the fast time response (< 100 ns) which is required by the acoustic microscope. In addition to detecting thermal phonons, we have also fabricated a bolometer next to an acoustic transducer and measured the coherent acoustic radiation at 8.0 GHz. Figure 5(c) shows how the bolometers will be employed in the fabrication of an acoustic lens. The bolometer is in a ring shape surrounding the acoustic transducer. Thus the phonons falling outside the transducer area will be detected by the bolometer. Therefore, it is possible to detect the echo from the sample both coherent, narrowband and incoherent, and broadband with this scheme.

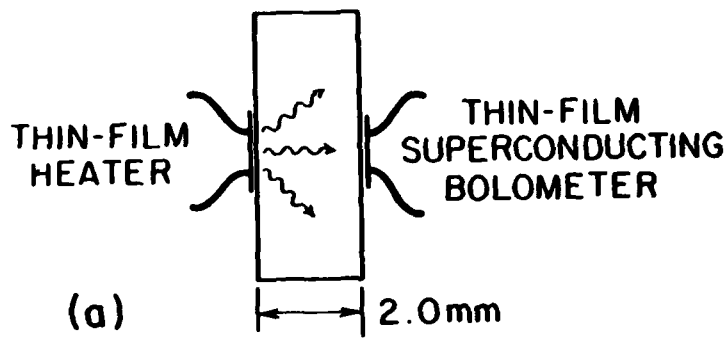

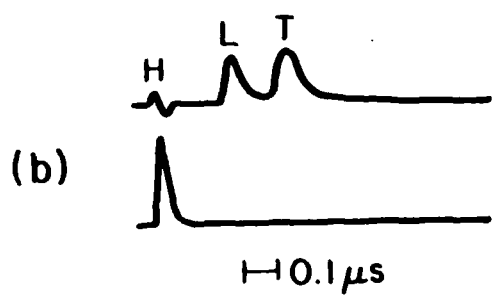

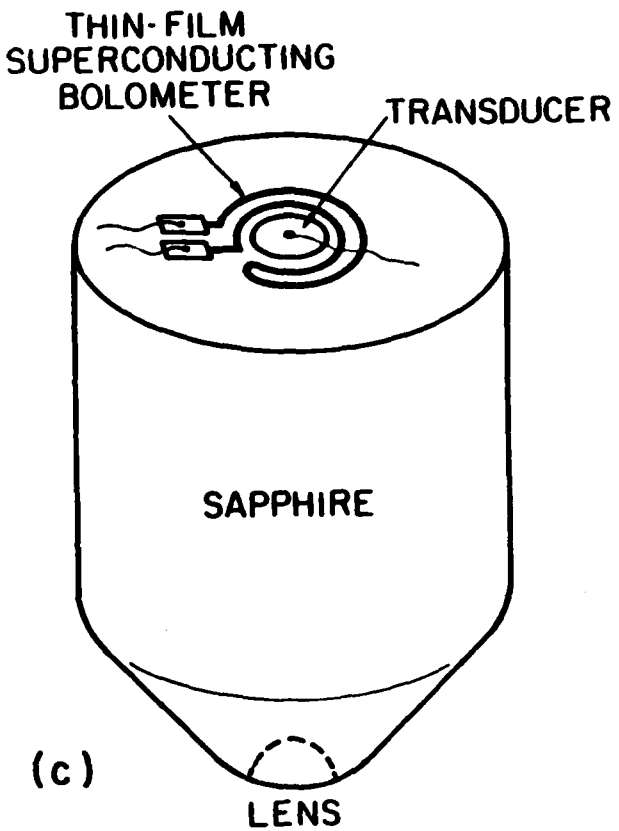

FIG. 5-- (a) The experiment for detection of thermal phonons from a thin-film heater using a superconducting bolometer. (b) An oscilloscope trace showing the detected longitudinal and transverse phonons. (c) Diagram of the bolometer-acoustic transducer configuration to be used on the acoustic lens.

C. Pressurized Helium

The signal-to-noise ratio of the acoustic microscope can be increased very simply by applying pressure to the superfluid helium which acts as the coupling fluid between the lens and sample. There is an effective attenuation of sound due to three-phonon processes in the liquid helium. This process, however, is very sensitive to the sound dispersion in the helium, which is, in turn, a function of pressure.

Figure 6 depicts a three-phonon scattering event in which two phonons collide and form a third phonon. (The reverse process also occurs.) The collision conserves energy and momentum. The phonon energy is $\hbar\omega$, and so conservation of energy requires $\omega_1 + \omega_2 = \omega_3$. The phonon momentum is $\hbar\vec{k}$, and so conservation of momentum requires $\vec{k}_1 + \vec{k}_2 = \vec{k}_3$. If there were no dispersion, i.e., $\omega = c_o k$ for all frequencies, and c_o is a constant speed, then the two conservation equations require that the phonons be collinear - all momenta in the same direction. If the dispersion is upward, as shown in Fig. 6, then the sound speed c is increasing with frequency. In this case, we see from the figure that the higher energy phonon ω_3 will have less momentum than the no dispersion case. Then, the two input phonons, ω_1 and ω_2 must intersect at a finite angle so that some of their momentum will be cancelled, and momentum will then be conserved. We thus see that the drawing in Fig. 6 is representative for the upward dispersion case. If the dispersion is downward, the higher energy phonon ω_3 has too much momentum, which cannot be obtained from the ω_1 and ω_2. Hence, if the dispersion is downward, the three-phonon process cannot conserve energy and momentum and thus becomes quite unlikely.

We are fortunate that in superfluid helium, the dispersion is adjustable. At low pressures, the dispersion is upward, and so three-phonon collisions occur

THREE PHONON SCATTERING

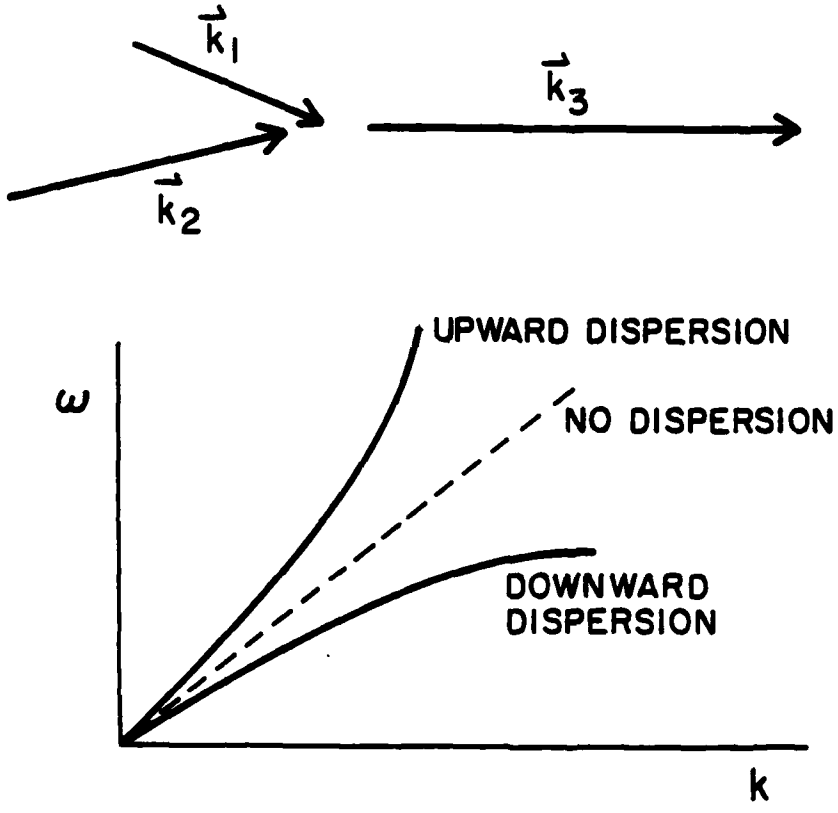

FIG. 6--Diagram showing the scattering of two phonons to form a third one for various dispersion cases.

at a finite angle. As pressure is applied, the dispersion becomes more linear and above 20 bar, the dispersion is downward. Hence, above 20 bar, the helium should be more transparent for sound, and the signal-to-noise should increase.

There is an additional change in helium when pressure is applied: several liquid parameters change such as the density, sound speed, and nonlinearity. All of these parameters shift the scattering amplitudes of the three phonon processes down as the pressure is increased, helping the signal-to-noise.

To test the pressure dependence of the signal-to-noise we placed an acoustic lens and a reflector in a pressure cell (Fig. 7). The cell has been previously described.[4] The cell allows the lens-sample spacing to be adjusted, and, of course, allows the application of pressure. In the experiment we measured the sound pulse which bounces off the reflector (flat sapphire) and returns to the acoustic lens. The received signal is plotted in Fig. 8 as a function of helium pressure in the cell for two frequencies with two different acoustic lenses. It can be seen that although the shape of the curve is considerably different between 7 and 8 GHz there is a large increase in signal-to-noise near 20 atmospheres as was expected from the arguments above.

D. Highly Nonlinear Acoustic Resonance - a New Result

At high pressures and high acoustic intensities, we expect the sound waves to generate many harmonics and form a converging shock wave. At this point, the sound intensity of the fundamental beam (which we measure) should saturate at a maximum value. This effect has been seen by many observers previously.[3] However, in our experiments - using very high frequency coherent sound in pressurized superfluid helium - we see a very different kind of behavior. The intensity of the reflected pulse of a sound beam actually can decrease as

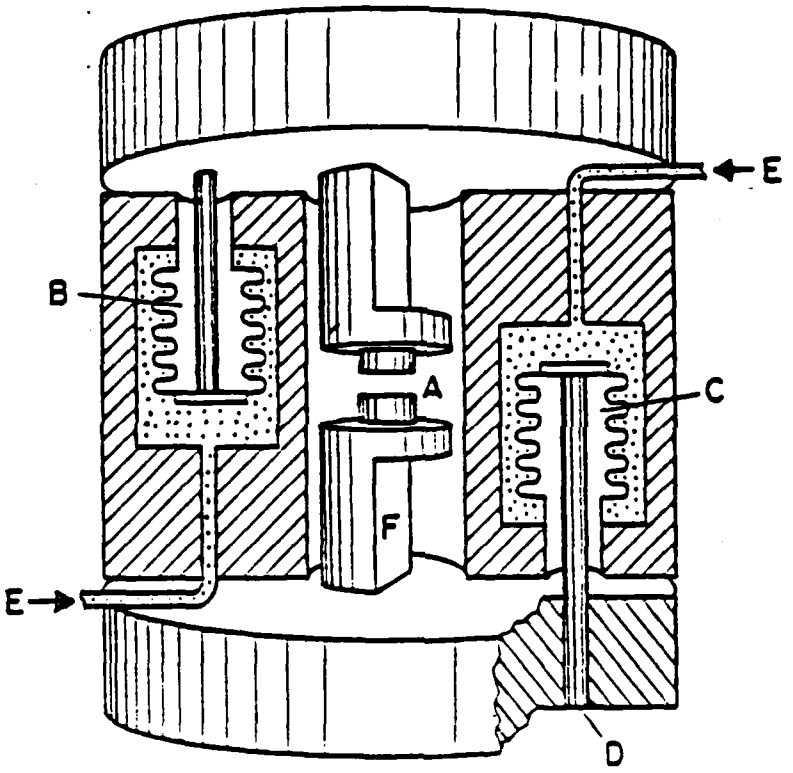

FIG. 7--Cutaway figure of the pressure cell.

A. Sapphire rods for the lens and the flat reflector.
B and C. Miniature bellows.
D. Pushrod.
E. Control capillaries.
F. Impedance matching circuitry.

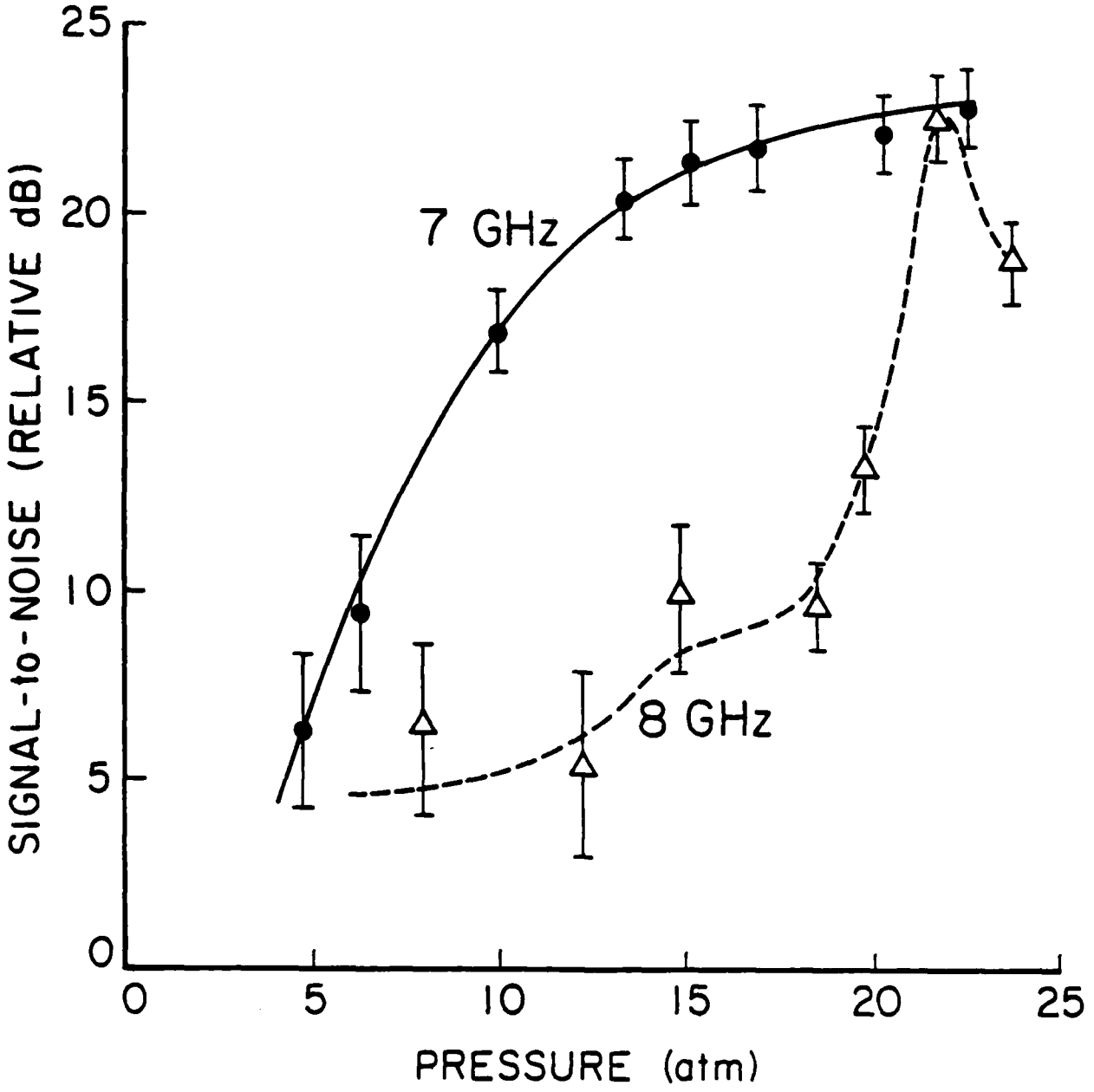

FIG. 8--Improvement of SNR upon pressurization of helium at frequencies of 7 and 8 GHz.

the input power is increased. We have seen this previously with plane waves.[5] We have performed two experiments at frequencies of 7 and 8 GHz with two different acoustic lenses to determine the behavior of high intensity sound wave propagation in case of focused beams.

Figure 9 shows the received power from an acoustic lens at 7 GHz focused on a flat sample. As the lens-to-sample spacing is varied, the power changes. At the peak power, the lens is said to be in focus. At low pressures, the qualitative shape of the curve is the same independent of the input acoustic power (Fig. 9(a)). The shape is relatively unchanged as we go to pressures greater than 20 bar if we keep the input power low. But when the input power is turned up and the helium pressure is high, the shape of the focus changes dramatically (see Fig. 9(b)). The curve shows some kind of resonant behavior where the received power oscillates with lens-to-sample spacing. Note this behavior only occurs when the sample is pulled away from the normal geometrical focus.

In the second experiment that we performed the frequency was 8 GHz and we used a different lens which was identical to the 7 GHz lens in terms of mechanical dimensions. The received power as a function of sample position is plotted in Fig. 10 for low and high pressures and different input power levels. It can be seen that the behavior is quite different in this case. At low power levels the received power is quite regular with one peak at the focus and nothing else at both positive and negative z positions at both low and high pressures. At high input levels we see another peak appearing at positive z at low pressures. At high pressures and high input levels, we see the main peak shifting towards positive z positions and smaller peaks appearing as the sample is moved away from the lens. We don't find the "oscillatory" behavior observed at 7 GHz. We believe that differences in the positioning of the transducer on the sapphire substrate

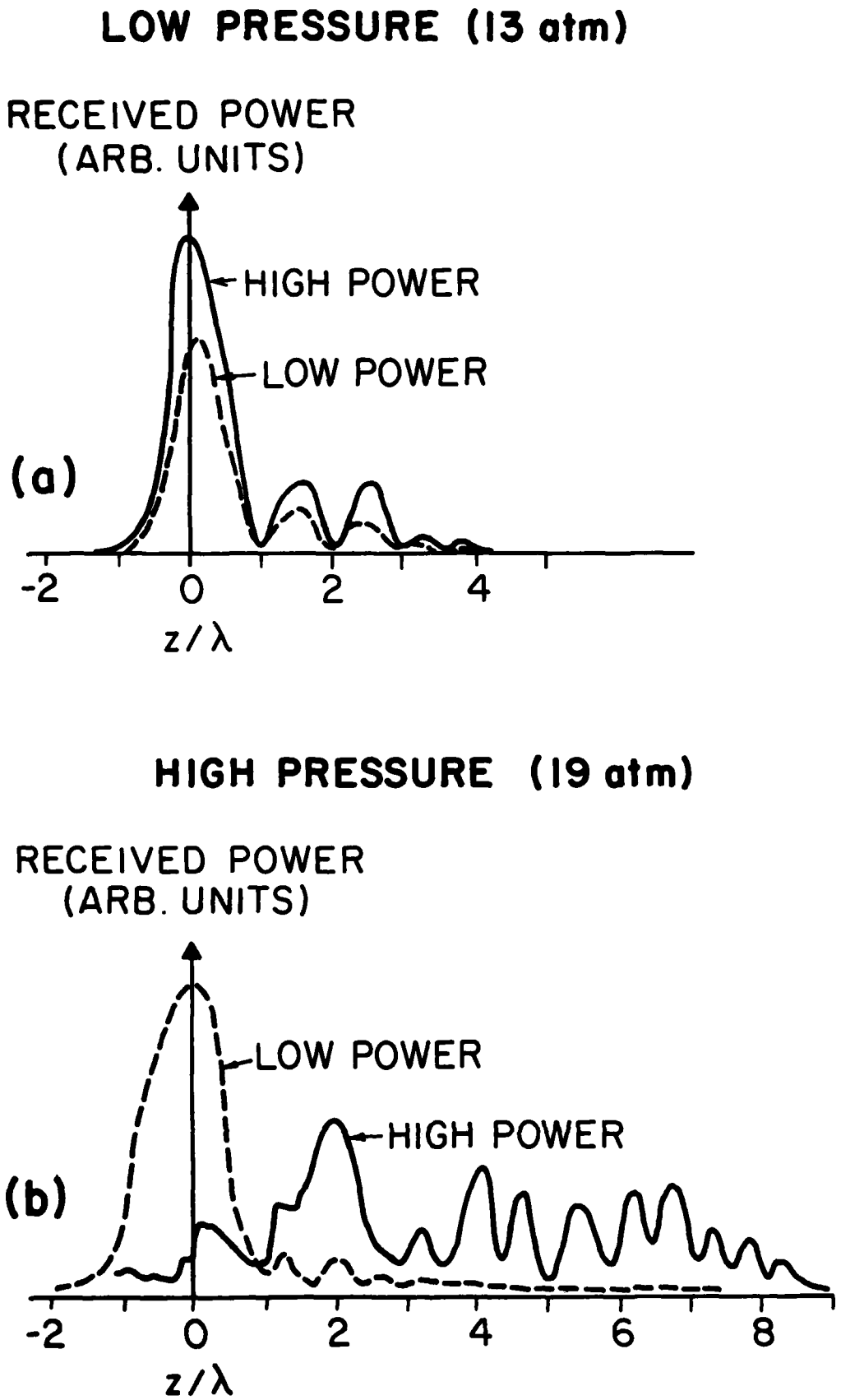

FIG. 9--V(z) curves at 7 GHz. Positive z corresponds to moving away from lens. (a) At low pressures, increasing power has little effect on shape. (b) At high pressures and high powers, V(z) has extended structure several wavelengths beyond focus.

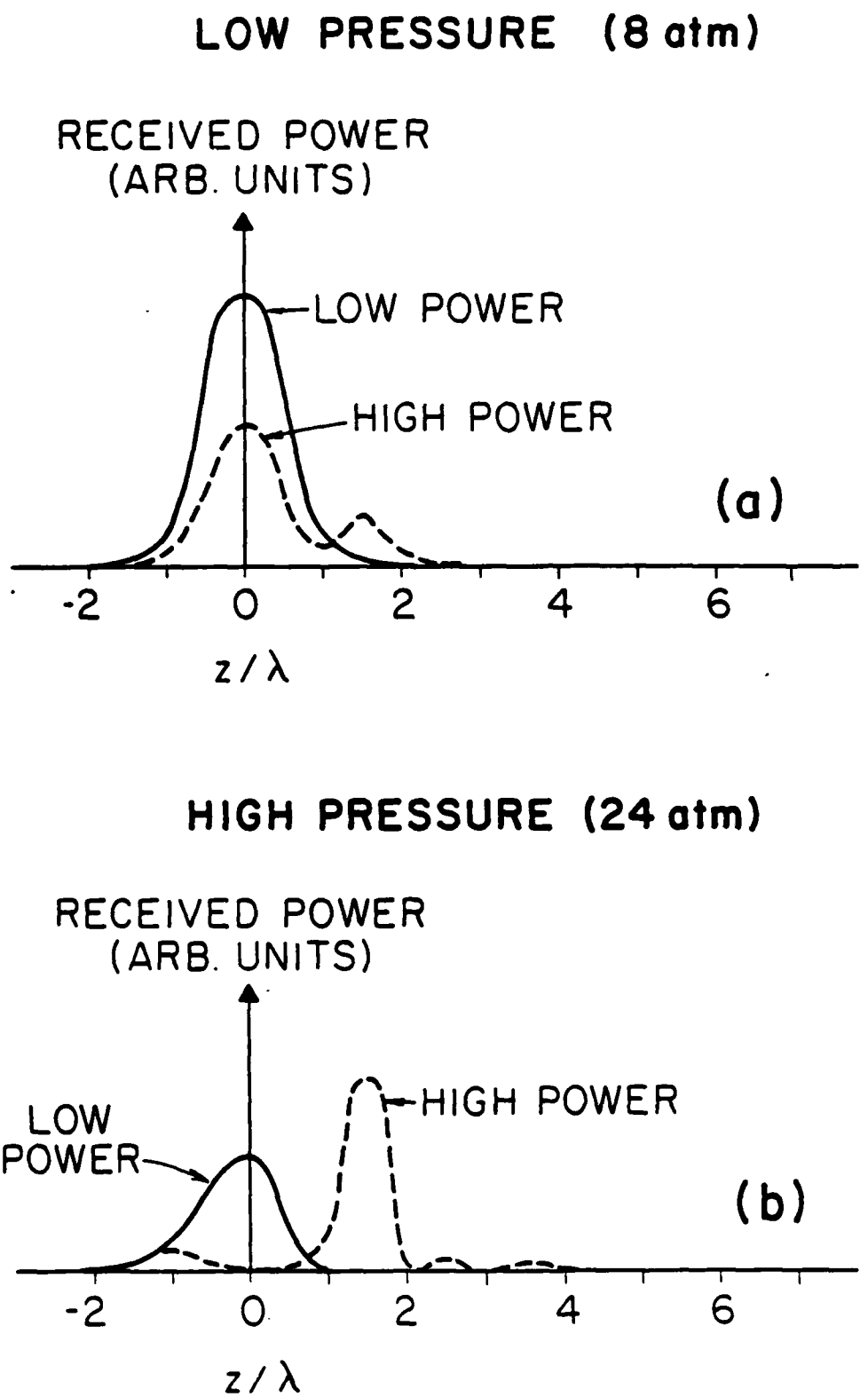

FIG. 10--V(z) curves at 8 GHz. (a) At low pressures, increasing the input power reduces the received power with little effect on shape. (b) At high pressures, increasing input power increases the received power and shifts the main peak.

which changes the illumination of the acoustic lens by the sound beam may be responsible for the different behavior observed in the two experiments. We will continue the study of this effect. It bears directly on the strength of the signal that we can expect from the acoustic microscope. It will as well indicate how well we have done with the design of our lens system.

E. Parametric Amplification

We have attempted, without success, to make an acoustic parametric amplifier in superfluid helium. The goal is two-fold: to increase the signal-to-noise by significantly decreasing the noise of the receiving system (by approximately 10 dB) and to further our understanding of resonant three-phonon processes in helium.

The key physical process in parametric amplification is stimulated decay. Figure 11 shows the process with a "pump" phonon colliding with the "signal" phonon. The signal phonon effectively stimulates the pump to decay into two phonons, one which looks like the signal, and the "idler" phonon which is determined by conservation of energy and momentum. We see in this process that the signal has gain (it has doubled in number of phonons) and the pump has depleted. If the pump is very large, the signal will grow exponentially from parametric amplification.

The noise of the parametric amplifier is determined by the number of phonons in the superfluid helium which are similar to the signal phonons. Those include thermal phonons and zero-point phonons which can also be thought of as quantum noise. For our experiments, the temperatures are so low that the thermal noise can be disregarded and the quantum noise dominates. Therefore, an acoustic parametric amplifier in low temperature superfluid helium would have nearly the lowest noise possible, more than a factor of 10 less than

PARAMETRIC AMPLIFICATION

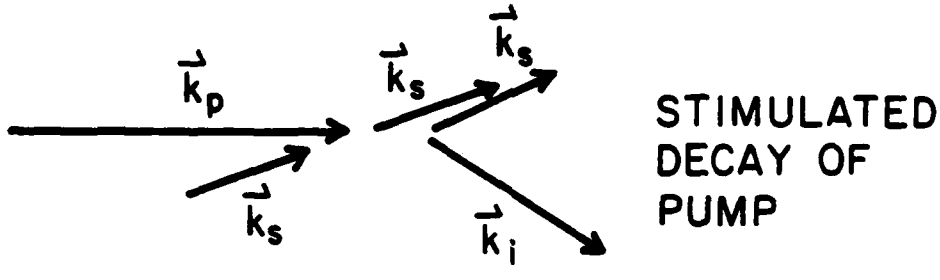

FIG. 11--Diagram showing stimulated decay of pump phonon by interaction with signal phonon, resulting in amplification of signal.

what we are presently using.

The designs that we have tried have not given us the results that we had planned for. The short wavelengths that we are using impose severe requirements on the alignment procedures and we are not yet in a position to meet these requirements.

II. MECHANICAL SCANNING

The acoustic microscope uses mechanical scanning to move the lens in relation to the sample and form an acoustic image. If the mechanical scanning of the microscope were perfect, the resolution of the microscope would be determined by the diffraction limit of the focused sound beam. Since we would like to have a resolution better than 100 Å, the mechanical scanning must be even more accurate. However, the scanner must also be capable of moving over a wide field of view (e.g. 10-20 μm). Coarse motion over centimeter distances is also desired to find a specific point on a sample and to move from one object to another. The scanner must also be capable of withstanding pressures of up to 24 atmospheres. This is required because of the considerable increase in the signal-to-noise ratio at such pressures.

The scanner previously used in the superfluid helium acoustic microscope[6] had problems with both accuracy and field of view. A moving coil-fixed magnet combination was used both to drive as well as sense motion. The system was not very rigid and room vibrations limited the accuracy to about 100 Å. The maximum field of view was approximately 100 μm, limited by the ohmic heating in the superconducting scanning coils. Therefore, only a small area on one sample could be imaged in a single cooldown. This scanner also could not be pressurized as it was not sealed on top to allow changing samples in the top

loading dilution refrigerator.[6]

We are approaching the above problems with a new design for the mechanical scanner, It has separate systems for fine and coarse motion laterally in X and Y directions. A third system will move it in the Z direction and move the samples in and out of focus. The scanner will be completely sealed to withstand high pressures required. Because of this, multiple samples will be placed in the scanner to allow imaging of several samples in a single cooldown.

In the new scanner fine motion with extreme accuracy will be obtained using stacked piezoelectric ceramics which have sub-Å accuracy. These ceramics have a maximum movement of 10-15 μm at room temperature. At liquid helium temperatures, however, the maximum motion is down by a factor of almost 8. A mechanical amplification scheme must be employed in order to get the 10-15 μm fine scanning required. The system must also be rigid so as not to introduce vibrations that will degrade the accuracy of the scanner. A mechanical scanner that satisfies these requirements has been developed at the National Bureau of Standards by Scire and Teague.[7] We have built scanners similar to theirs by modifying some dimensions of the original scanner to satisfy the space requirements of our helium microscope. Figure 12 shows a diagram of the fine scanners and the way it achieves mechanical amplification. With the dimensions used we expect to get an amplification of approximately a factor of 20. We have tested the scanners that we built and found out that the amplification factor was only 2.5 at room temperature. The difference between the theoretical and experimental values is probably due to the critical dimensions required. We expect to improve on this in the near future. We have also tested the stage at liquid nitrogen temperatures and measured an amplification factor of 4 . Therefore, we expect to have a range of at least

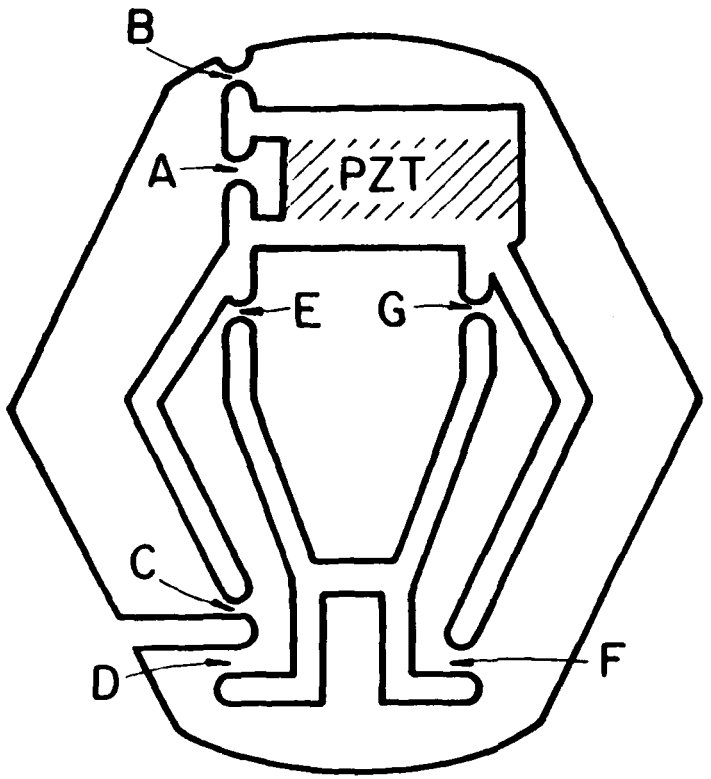

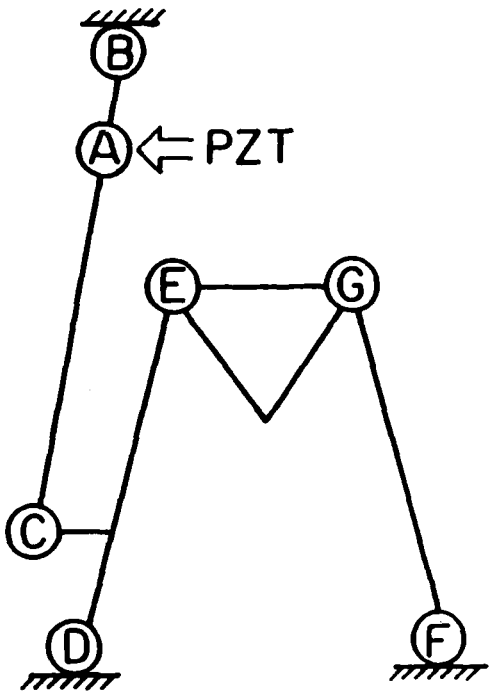

$$\text{Magnification} = M_1 \; M_2$$

$$M_1 = 1 + \frac{|A - C|}{|A - B|}$$

$$M_2 = 1 + \frac{|C - E|}{|C - D|}$$

FIG. 12--Top view of the fine scanner and principles of operation of the scanner.

4 μm with these scanners at liquid helium temperatures. This would represent a movement over several hundred spot diameters and this is sufficient to produce quality images.

Two of the scanners mentioned above will be stacked up to achieve fine motion in X and Y directions. The fine scan in Z direction will be obtained using a simple ½ inch long piezoelectric tube as only 1-2 μm of motion is required in this direction.

Coarse motion with the accuracy and stability that we require is a difficult problem, as evidenced by the engineering troubles with the vacuum tunneling microscope. Compounding our problem is the low temperature environment and low heat dissipation requirement of the helium acoustic microscope. We are now constructing a system that incorporates electric motors, heavily geared down to provide motion in steps of thousands of angstroms.

This scanner is the first of its kind and we expect to have some problems in the initial design. For a beginning we have built a simplified scanner that will enable us to observe these problems and correct them in the final design. A schematic diagram of this scanner is shown in Fig. 13. Coarse motions in X and Y directions are not available in this design and only coarse Z motion is provided to bring the sample in and out of focus. The lens and matching network is connected to the X, Y and Z fine motion assembly mentioned above. This assembly is secured between four rods which are mounted on the bottom of the cell. An electric motor is also located on the bottom of the cell to provide coarse motion. A planetary gear assembly is connected to the shaft of the motor on top. The gearbox has a final ratio of 4000:1 and is used to increase the torque of the motor and to limit the motion of the sample plate. The sample plate is located on top of the gearbox and can slide up and down between the four rods mentioned previously. The plate is coupled to the gearbox via a screw

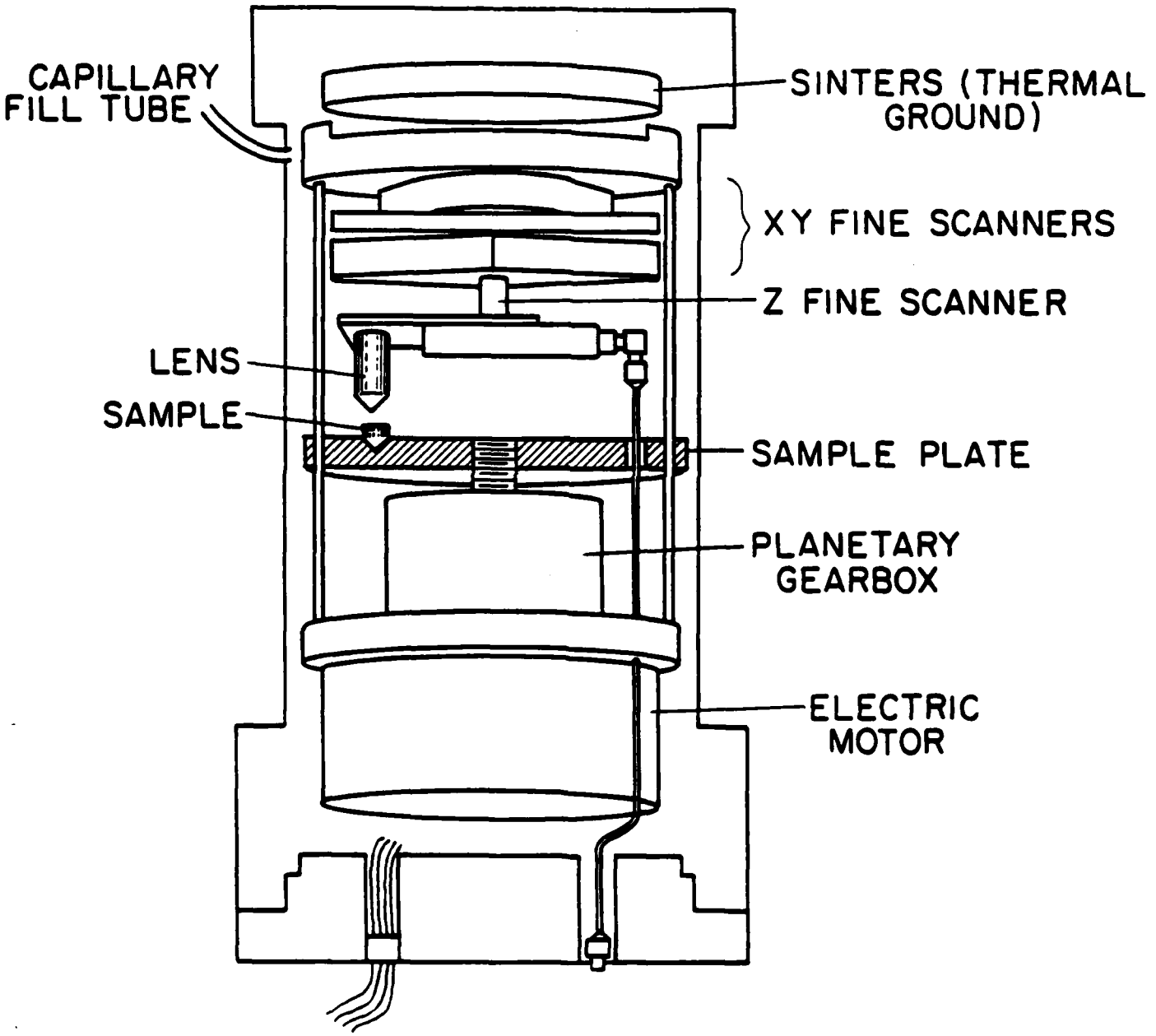

FIG. 13--Cutaway view of the complete scanner assembly.

which converts the rotational motion of the gears to up-down motion.

The electric motor is the important part of the coarse motion. It must provide sufficient torque to turn the gears. It must work after degreasing and it must be easily rewindable with superconducting wires. It also must be small enough to fit into the limited space available. We have tried dc stepping motors in the scanner, but they did not have enough torque. They were unreliable at low temperatures. We are now using ac synchronous motors which do provide sufficient torque and they seem to work well at low temperatures. They will be rewound with niobium wires to decrease heat dissipation in the coils.

We are now in the final stages of testing this scanner and soon we should be able to image with it. In the final design we will use alternate designs for the motor and a linear induction motor to provide motion in θ and R directions (instead of X and Y).

REFERENCES

1. J. S. Wang and K. M. Lakin, Proceedings of 1982 IEEE Ultrasonics Symposium, 480 (1982).
2. P. Ruden and G. H. Döhler, Solid State Comm. 45, (1), 23 (1983).
3. D. Rugar, J. Appl. Phys. 56, (5), 1338 (1984).
4. D. Rugar and J. S. Foster, Phys. Rev. B, 30, (5), 2595 (1984).
5. J. S. Foster and S. Putterman, Phys. Rev. Lett. 54, (16), 1810 (1985).
6. J. S. Foster, Ph.D. Dissertation, Stanford University (1984).
7. F. E. Scire and E. C. Teague, Rev. Sci. Instrum. 49, (12), 1735 (1978).

FMD

12-86

DTIC